Arabian Journal of Chemistry (2016) 9, 179–189

King Saud University

Arabian Journal of Chemistry

www.ksu.edu.sa
www.sciencedirect.com

ORIGINAL ARTICLE

Meso- and macroporous sulfonated starch solid acid catalyst for esterification of palm fatty acid distillate

Ibrahim M. Lokman [a,b,c], **Umer Rashid** [d,*], **Yun Hin Taufiq-Yap** [a,b,e,*]

[a] *Catalysis Science and Technology Research Centre, Faculty of Science, Universiti Putra Malaysia, 43400 UPM Serdang, Selangor, Malaysia*
[b] *Department of Chemistry, Faculty of Science, Universiti Putra Malaysia, 43400 UPM Serdang, Selangor, Malaysia*
[c] *School of Chemistry, Faculty of Applied Sciences, Universiti Teknologi MARA, 40450 Shah Alam, Selangor, Malaysia*
[d] *Institute of Advanced Technology, Universiti Putra Malaysia, 43400 UPM Serdang, Selangor, Malaysia*
[e] *Curtin Sarawak Research Institute, Curtin University, 98009 Miri, Sarawak, Malaysia*

Received 17 May 2015; accepted 26 June 2015
Available online 2 July 2015

KEYWORDS

Meso- and macroporous carbon;
Heterogeneous solid acid catalyst;
Physico-chemical characterization;
Esterification;
Biodiesel

Abstract In the present work, a heterogeneous solid acid catalyst was successfully developed from starch. The catalyst was prepared by a significant two-step process; the initial step was incomplete carbonization of starch (ICS) at 400 °C for 12 h and consequently followed by sulfonation process using concentrated H_2SO_4 to produce sulfonated-incomplete carbonized starch (ICS-SO_3H). The characterization of the ICS-SO_3H catalyst was done for chemical and physical properties such as X-ray diffraction (XRD), ammonia-temperature programmed desorption (NH_3-TPD), surface area analysis, thermal gravimetric analysis (TGA), elemental analysis and morphology analysis by scanning electron microscope (SEM). BET results showed the structure of ICS-SO_3H consists of meso- and macro-porous properties, which allowed high density of the $-SO_3H$ group attached on its carbon networks. The catalytic activity of ICS-SO_3H catalyst was determined by analyzing the catalyst performance to esterify palm fatty acid distillate (PFAD) and sequentially produced methyl ester. The maximum free fatty acid (FFA) conversion and FAME yield were as high as 94.6% and 90.4%, respectively, at 75 °C using 10:1 methanol-to-PFAD molar ratio and 2 wt.% of catalyst within 3 h. The catalyst has sufficient potential to recycle up to 6 reactions without

* Corresponding authors at: Catalysis Science and Technology Research Centre, Faculty of Science, Universiti Putra Malaysia, 43400 UPM Serdang, Selangor, Malaysia. Tel.: +60 3 89466809; fax: +60 3 89466758 (Y.H. Taufiq-Yap). Tel.: +60 389467393; fax: +60 389467006 (U. Rashid).
E-mail addresses: umer.rashid@yahoo.com (U. Rashid), taufiq@upm.edu.my (Y.H. Taufiq-Yap).

Peer review under responsibility of King Saud University.

Production and hosting by Elsevier

http://dx.doi.org/10.1016/j.arabjc.2015.06.034

reactivation step and any remarkable loss of catalytic activity. It revealed that the heterogeneous ICS-SO_3H catalyst exhibits high stability, reusability and catalytic activity.

1. Introduction

Recently, great concern has been discussed on the exhaustion of fossil fuel resources and the environmental pollutions due to the fuel's combustion. Nowadays, the energy is distributed into three basic economic needs, which are for the electric power technologies, process heating for industries and consumer, and thirdly, for the private and cargo transportations (Ashnani et al., 2014; Reynolds, 2014). Therefore, the critical development of renewable alternative fuels has now become important. Biodiesel has attracted high attention as a substitute fuel for fossil diesel, due to it being environmentally benign and having almost similar functional properties as fossil diesel. The energy released from biodiesel was larger than the energy produced from petroleum diesel – which was expected to provide a great benefit to the society (Cho et al., 2013). In general, biodiesel or scientifically known as fatty acid methyl ester (FAME) can be produced by transesterification or esterification of renewable sources such as vegetable oils and animal fats (Alhassan et al., 2013; Lee et al., 2011; Lokman et al., 2014a; Mekhilef et al., 2011; Rashid et al., 2011a,b; Taufiq-Yap et al., 2011). In the recent years, Malaysia has been producing roughly 700,000 metric tons of PFAD annually as by-product from refinery process of crude palm oil (Ping and Yusof, 2009). PFAD had been classified as a cheaper low quality grade feedstock due to its high FFA content (>85 wt.%). Therefore, the homogeneous and heterogeneous alkaline catalysts are prohibited for transesterification of PFAD to avoid saponification process caused by neutralization of FFA (Atadashi et al., 2012). Nevertheless, the heterogeneous solid acid catalyst is more sensible for the production of biodiesel due to high FFA feedstock.

It is important to note that heterogeneous solid-acid catalyst can efficiently separate from the product by simple decantation or centrifugation process. It allows more environmental friendly biodiesel production process by reducing the corrosive matter problems and enables the potential of continuous process (Islam et al., 2013). There are a few numbers of heterogeneous solid acid catalysts that have been evaluated for biodiesel production, *i.e.*, activated carbon-supported tungstophosphoric acid catalyst (Badday et al., 2013), ferric alginate–Lauric acid (Peng-Lim et al., 2012), ferric hydrogen sulfate (Alhassan et al., 2013) and Aminophosphonic acid resin D418 (Liu et al., 2013). Unfortunately, the preparation costs and steps are both expensive and complicated (Okuhara, 2002). Recently, a novel carbon solid acid catalyst derived from incomplete carbonized carbohydrate had recently been described. This catalyst gained much attention due to the low-cost production, easy preparation process, high effectiveness, greener and suitable for esterification of waste oil containing high FFA (Chin et al., 2012; Dashmane et al., 2013; Ormsby et al., 2012; Wang et al., 2013). Also popularly known as sugar catalyst, it is one of the amorphous carbon materials that consists of small polycyclic aromatic carbon sheets (Okamura et al., 2006); highly potential to be incorporated with high amount of sulfonic (—SO_3H) groups, despite the low surface area and porosity – which might hinder the diffusion of reactant to active sites (Yu et al., 2008).

Significant researcher have been highlighted for the porous support materials as they are particularly useful for every application that requires the fast and efficient reaction, for instance energy storage, drug delivery, chemical sensing and catalysis (Stein et al., 2008; Walcarius and Collinson, 2009). In application of biodiesel production, the larger pores catalyst provides easy access of the reactant to the active sites of the catalyst; this will give advantage for selectivity and increase the reaction speed (Fratzl and Weinkamer, 2007). Carbohydrate-derived solid acid catalysts have low surface area and consist of porous carbon structure. Hence, slight increase in larger surface area and pores diameter could increase the overall performance of the catalyst, which may be suitable for biodiesel production.

Herein, we demonstrated the preparation of meso- and macro-porous carbon-based solid acid catalyst from starch as carbon precursor to increase the activity of the catalyst. The catalyst was synthesized by sulfonation of incomplete carbonized starch (ICS) to produce sulfonated-starch solid acid catalyst (ICS-SO_3H). The ICS-SO_3H was characterized in a detailed manner using X-ray diffraction (XRD), ammonia-temperature programmed desorption (NH_3-TPD), BET surface area analysis, thermal gravimetric analysis (TGA), Raman spectroscopy, CHNOS elemental analysis and morphology analysis by scanning electron microscope (SEM). PFAD was chosen as the test oil in this work and the effect of different operating parameters such as methanol molar ratio, catalyst amount, reaction temperature and reaction time was intensively studied for esterification of PFAD. The studies on reusability of the catalyst and leaching of active sites were also appraised.

2. Experimental details

2.1. Chemicals and materials

PFAD was supplied by Jomalina oleochemical RandD, Sime Darby Sdn. Bhd. (Klang, Selangor). Commercial grade starch was purchased from Sigma–Aldrich. Sulfuric acid (H_2SO_4), hydrochloric Acid (HCl) and potassium hydroxide (KOH) were purchased from J.T. Baker. The solvents such as methanol (95%), ethanol (95%) and analytical grade *n*-hexane (99.9%) were obtained from Merck chemical company. FAME standards for chromatography analysis including methyl oleate, methyl palmitate, methyl linoleate, methyl myristate, methyl stearate and methyl heptadecanoate were obtained from Fluka.

2.2. Feedstock analysis

The physico-chemical properties of PFAD feedstock were analyzed according to AOCS, ISO and BS standard methods.

2.3. Catalyst preparation

15 g of starch was heated at 400 °C for 12 h with N_2 gas flow. The resultant black carbon ICS was then milled to a powder for 1 h at 1000 rpm. For activation process, approximately 5 g black powder was suspended in 200 mL of concentrated H_2SO_4 and refluxed at 160 °C for 12 h in inert environment, to introduce $-SO_3H$ on the surface and pore of the catalyst. The suspension was then diluted with 500 mL of distilled water and filtered. The ICS-SO_3H catalyst was subsequently washed repeatedly with hot distilled water to remove all excesses of sulfate ions until pH of the filtrate is the same as the pH of wash water. The ICS-SO_3H catalyst was collected and dried at 80 °C for 24 h to remove excess moisture.

2.4. Catalyst characterization

The synthesized ICS-SO_3H catalyst was characterized and analyzed in detail. The robust structure of the carbon catalyst was determined by X-ray diffraction (XRD) (Shimadzu, XRD 6000) with the scanning range of 2 theta (θ) from 2° to 60° at a scanning rate of 4° min^{-1}. Fourier transform infrared (FT-IR) spectroscopy (Perkin Elmer, 1725 X) was used to characterize the functional groups of the catalyst, scanned from 500 to 4000 cm^{-1}. Raman spectroscopy (WITec, Alpha 300R) micro-imaging was applied to analyze the graphitic structure of the catalyst. The thermal stability of the catalyst was analyzed by thermal gravimetric analyzer equipped with differential gravimetric analysis (TGA–DTG) (Mettler, Toledo 990). The sample's weight loss was recorded and analyzed to determine the stability of the catalyst samples.

A morphological study of the catalysts has been performed by using scanning electron microscopy (SEM) (JEOL, JSM-6400). The textural properties such as the surface area, pore volume and pore radius were determined by N_2 adsorption–desorption analysis, Brunauer–Emmett–Teller (BET) and Barrett–Joyner–Halenda (BJH) (Thermo Finnigan, Sorptomatic 1990 series). The total amount and distribution of acid sites were analyzed by ammonia-temperature programmed desorption (NH_3-TPD) (Thermo Finnigan, TPDRO 1100 series equipped with thermal conductivity detector (TCD)). About 0.05 g sample was firstly pretreated at 150 °C for 1 h under N_2 flow, followed by adsorption of NH_3 for 1 h. The sample was again flowed by N_2 gas for 30 min. Finally, the sample was heated from 50 to 950 °C at 5 °C min^{-1} with helium flow as the carrier gas. The amount of the NH_3 gas desorbed from the catalyst throughout the heating process was plotted.

2.5. Esterification of PFAD oil

The esterification of PFAD was carried out by classical conventional reflux system. In typical run, a specific amount of PFAD was liquefied by heated at 70 °C. The preheated PFAD was poured into the 50 mL round bottom flask. The methanol and ICS-SO_3H catalyst were added and mixed with liquefied PFAD before it being heated at specified temperature. The mixture was stirred at 600 rpm throughout the experiment. A series of reactions were completed at different operating conditions: catalyst amount in the range of 1–5 wt.% of PFAD, methanol-to-PFAD molar ratio in the range of 5–25, reaction temperature in the range of 65–85 °C and reaction time from 1 to 5 h. Finally, production mixture was centrifuged at 4000 rpm for 10 min to separate the catalyst and later the liquid product was allowed to settle into two phases. The bottom layer containing FAME was collected and purified with distilled water before being analyzed by gas chromatography (GC). The excess upper-methanol layer was recovered by distillation and used for subsequent reaction.

2.6. Reusability and leaching analysis of catalyst

The esterification of PFAD over mesoporous ICS-SO_3H catalyst was carried out using 2 wt.% of catalyst. The optimum operating parameters were kept constant in every reaction cycle with 10:1 methanol-to-PFAD molar ratio, 75 °C reaction temperature, and 2 h reaction time. The production mixture was centrifuged at 4000 rpm for 10 min. The sediment or catalyst was collected, washed with *n*-hexane and dried at 80 °C for next reaction cycle. Meanwhile, the biodiesel product on each cycle was collected for determination of FAME yield by GC analysis and detection of $-SO_3H$ group using CHNOS elemental analysis for leaching analysis.

2.7. PFAD methyl ester analysis

The FFA conversion of oil was determined by the following (AOCS 5a-40) standard method as Eq. (1), where, AVf and AVp were assigned for acid value of feedstock and product, respectively.

$$\%\text{FFA conversion} = \frac{AV_f - AV_p}{AV_f} \times 100 \quad (1)$$

The analytical FAME yield of the product was measured by GC-FID (Shimadzu, GC-14C, Japan). It was equipped with highly polar capillary column BPX 70, SGE Company (length; 30 m, ID; 0.25 mm and capillary 0.25 μm). The GC was programmed as follows: The GC injector port and detector temperature were set at 230 °C and 270 °C, respectively. The GC oven was programmed with the rising temperature, starting from 100 °C up to 250 °C at a rate of 10 °C min^{-1}. Helium gas was used as the carrier gas and *n*-Hexane (99.9%) was used as the solvent. The 500 μg mL^{-1} of 5 reference FAME standard solutions including methyl oleate, methyl palmitate, methyl myristate, methyl linoleate and methyl stearate were prepared and injected into the injector port for the standard reference. Meanwhile, biodiesel product was diluted with *n*-hexane containing 500 μg mL^{-1} of methyl heptadecanoate (internal standard solution). 1 μL of sample was injected into the GC injector port. The FAME yield of the product was calculated according to Eq. (2) as follows:

$$\%\text{yield of FAMEs} = \frac{W_{\text{FAMEs}}}{W_{\text{raw material}}} \times 100 \quad (2)$$

where W_{FAMEs} and $W_{raw\ materials}$ stand respectively for the weight of the FAME produced and weight of starting materials used.

The methyl ester sample was analyzed by using a Shimadzu QP2010 Plus gas chromatography equipped with a capillary column of RTX-65 (30 m, 0.25 mm ID, 0.25 μm) and a mass spectrometer as detector.

3. Results and discussions

3.1. PFAD feedstock analysis

Table 1 shows the physical characteristics and properties of the PFAD feedstock. Calculations to determine the values of the FFA content, acid and saponification value, conventional mass per volume and fatty acids were carried out using the AOCS and ISO Test Methods. The iodine value (IV) was used to find out the total unsaturation in PFAD feedstock. The IV of the sample was 0.523 ± 1.62 g g^{-1} of sample. Meanwhile, the average molecular weight of the sample was 235 ± 5.4 g mol^{-1}, which was derived from the saponification value (149.74 ± 4.72 mg KOH g^{-1} sample). The average acid value and FFA content were 172.6 ± 3.53 mg KOH g^{-1} of PFAD and 86.3 ± 2.45%, respectively. The major components of fatty acid in the PFAD were palmitic ($C_{16:0}$) and oleic ($C_{18:1}$) acids, which were 45.7 ± 1.32 wt.% and 40.2 ± 1.21 wt.%, respectively.

3.2. Characterization of ICS-SO_3H catalyst

X-ray diffraction analyses of the starch catalyst before and after sulfonation are given in Fig. 1. The catalyst exhibited both broad and weak diffraction peaks at 2Θ = 10–30° and 2Θ = 35–50° for both samples, which were assigned for the existence of graphitic (002) and (101) planes, respectively. Both peaks indicated presence of amorphous carbon structure that consists of polycyclic aromatic carbon ring oriented in considerable random fashion. A definite C(101) plane is due to the existence of the *a* axis of the graphite structure. It

Table 1 Characteristics and properties of PFAD feedstock.

Properties (unit)	Methods	PFAD
Iodine value, Wijs (g/100 g)	BS 684	52.3 ± 1.62
FFA (%)	AOCS Ca 5a-40	86.3 ± 2.45
Acid value (mg KOH/g of sample)	AOCS Ca 5a-40	172.6 ± 3.53
Conventional mass per volume at 50 °C (kg/l)	ISO 6883 (1995)	0.8634 ± 1.63
Water content (wt.%)		0.089 ± 0.004
Saponification value (mg KOH/g of sample)	AOCS Tr 1a-64	149.74 ± 4.72
Unsaponifiable matter (wt.%)	AOCS TK 1a-64	–
Average molecular weight (g/mol)		235 ± 5.4
Palmitic acid ($C_{16:0}$) (wt.%)		45.7 ± 1.32
Oleic acid ($C_{18:1}$) (wt.%)		40.2 ± 1.21
Linoleic acid ($C_{18:2}$) (wt.%)	AOCS Ce1-62	7.9 ± 0.21
Myristic acid ($C_{14:0}$) (wt.%)	and Ce-661	1.9 ± 0.05
Stearic acid ($C_{18:0}$) (wt.%)		4.3 ± 0.09

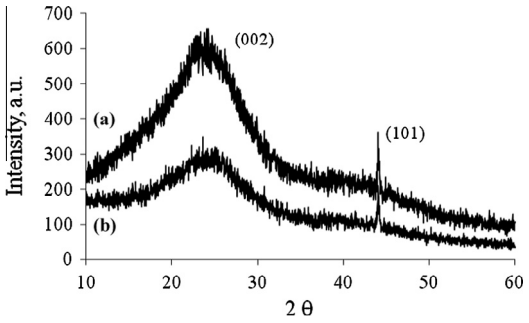

Figure 1 XRD analysis of (a) ICS and (b) ICS-SO_3H catalyst.

indicates the sample was composed by a high degree of carbonization with larger carbon sheets (Nakajima and Hara, 2007), which may be important for the catalyst activity during the esterification reaction process. The results were in agreement with the previous reports (Nakajima and Hara, 2007, 2012; Lou et al., 2008; Zong et al., 2007).

Infrared spectra of ICS and sulfonated-carbon catalyst, ICS-SO_3H are shown in Fig. 2. The strong absorption bands were observed at around 1700 cm^{-1} and 1590 cm^{-1} for both ICS and ICS-SO_3H catalysts; indicating the absorption of carbonyl, C═O and aromatic C═C carbon structure, respectively. The presence of symmetric and asymmetric C—O—SO_3H functional groups for ICS-SO_3H catalyst was detected by the strong absorption bands that had occurred at 1030 cm^{-1} and 1140 cm^{-1} stretching vibrations (Guo et al., 2012). Meanwhile, the weak absorption bands identical to the S═O symmetric and asymmetric were also observed for ICS sample – this is due to the IR absorption ability of the carbon (C—C) catalyst's framework (Lokman et al., 2015).

The Raman spectra of starch catalyst before and after the acid activation are depicted in Fig. 3. The spectra exhibited two distinct bands: D-band at 1350 cm^{-1} which was assigned for the defects in the sheets of carbon structure, and G-band at 1580 cm^{-1} which was commonly attributed to the vibrations of opposite direction of carbon atom of single crystal – normally it is high for graphitic materials (Shu et al., 2010). From this result, it was observed that both carbon structures of the catalyst consist of partially graphitic carbon structure with the amorphous carbon in the bulk of the carbon catalysts.

The thermal stability of the carbon-based solid catalysts before and after sulfonation was examined by TGA–DTG analyzer as shown in Fig. 4. The decomposition pattern shows

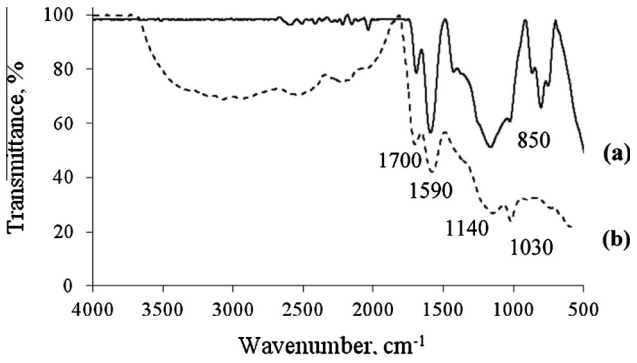

Figure 2 IR spectra of (a) ICS and (b) ICS-SO_3H catalyst.

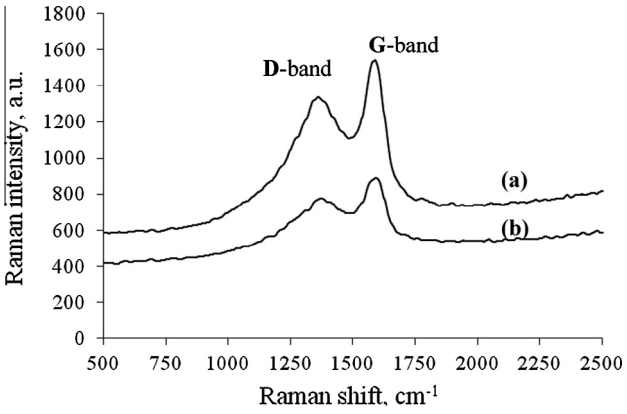

Figure 3 Raman spectra of (a) ICS and (b) ICS-SO_3H catalyst.

two stages of weight loss for the ICS sample (Fig. 4a) starting from 300 to 1000 °C due to decomposition of more than 50 wt.% of carbon structure that consists of C—O and C—C bonding. Meanwhile, Fig. 4(b) shows another two stages of weight loss (around 10 wt.%) starting from 200 to 450 °C that indicated the decomposition of carboxylic group, COOH and sulfonic, C—O—SO_3H functional groups for the ICS-SO_3H catalyst. Zong et al. (2007) reported the TGA–DTG curve of amorphous carbon catalyst derived from sugar (D-glucose) – it was similar and in good agreement with our present result.

Fig. 5 shows the NH_3-TPD profile of starch catalysts before and after sulfonation. One distinct NH_3 desorption peak was observed for the ICS (Fig. 5a) at 400–900 °C which maximized at 550 °C. Meanwhile, two distinct NH_3 desorption peaks were observed for ICS-SO_3H catalyst (Fig. 5b). The first peak,

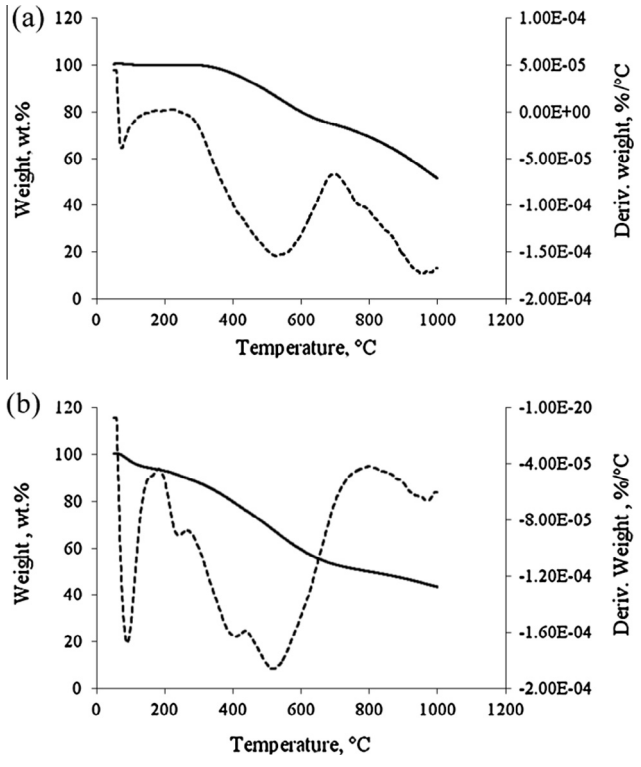

Figure 4 TGA of catalyst (a) ICS and (b) ICS-SO_3H catalyst.

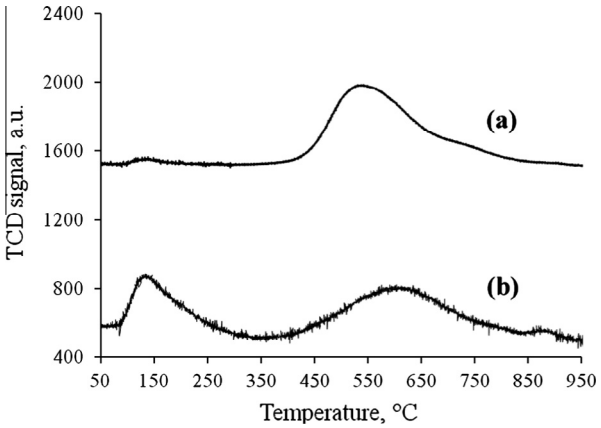

Figure 5 TPD-NH_3 analysis of (a) ICS and (b) ICS-SO_3H catalyst.

which was in range of 100–350 °C maximized at 150 °C, had been assigned for weak Brønsted acid site. In contrast, the second peak that was in the range of 350–950 °C maximized at 600 °C, had been ultimately assigned for strong Brønsted acid site. A peak was detected at a lower temperature for ICS-SO_3H catalyst, which corresponds to the presence of the sulfonic group as determined by the TGA in Fig. 4(b). Shu et al. (2010) reported the similar NH_3-TPD profile for the sulfonated carbon based acid catalyst derived from the vegetable oil asphalts.

Fig. 6 shows the SEM image of ICS-SO_3H catalyst. It was observed that the average size of grain particles was greater than 10 μm. The incomplete carbonized starch exhibited a loose irregular network structure – similar to the ones reported by Takagaki et al. (2007) and Nakajima and Hara (2007). The Brunauer–Emmet–Teller (BET) surface area analysis was carried out to analyze the surface characteristics of the starch catalyst in detail. Fig. 7 shows the N_2 adsorption–desorption isotherms of ICS (Fig. 7a) and ICS-SO_3H (Fig. 7b) catalyst. In our observation, both graphs show typically type-V, where there is a small adsorbate–absorbent interaction associated with the pores in the 1.5–100 nm ranges. The existence of hysteresis loops, which was nitrogen condensation step occurred at high P/P_o around 0.9–1.0, indicating the presence of multimodal with narrow and broad pore distribution. Hysteresis indicates the capillary condensation in meso- and macro-pores (Kim et al., 2010; Zhao and Collinson, 2010). In Fig. 7(a) the pore distribution pattern showed the ICS consists of mesopores (12–50 Å or 1.2–5 nm) with sharp peaks centered at 1.4, 2.0 and 3.3 nm. The presence of macropores was determined by the broad peak in the range of 90–1500 Å (9–150 nm) centered at 500 Å (50 nm). Furthermore, the prepared ICS-SO_3H catalyst has pore distribution in the range of 14–50 Å (1.4–5 nm) having sharp peaks centered at 1.6, 2.0, 3.2 and 4.5 nm, which were categorized as mesoporous carbon structure. The existence of broad peak in the range of 100–2000 Å equivalent to 10–200 nm centered at 50 nm indicates the presence of macropores (Valle-Vigón et al., 2012; Zhang et al., 2014, 2015). The calculated results from Barrett–Joyner–Halenda (BJH) show that the sample consists of bimodal porosity of meso- and macro-pores carbon slit with the average pore size of 43.7 nm and specific pore volume was 0.15 $cm^3\ g^{-1}$.

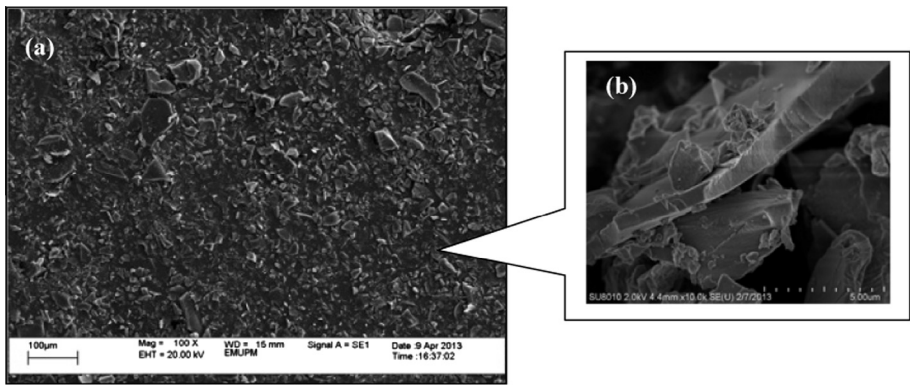

Figure 6 SEM images of ICS-SO_3H catalyst at (a) 100× and (b) 10,000× magnification.

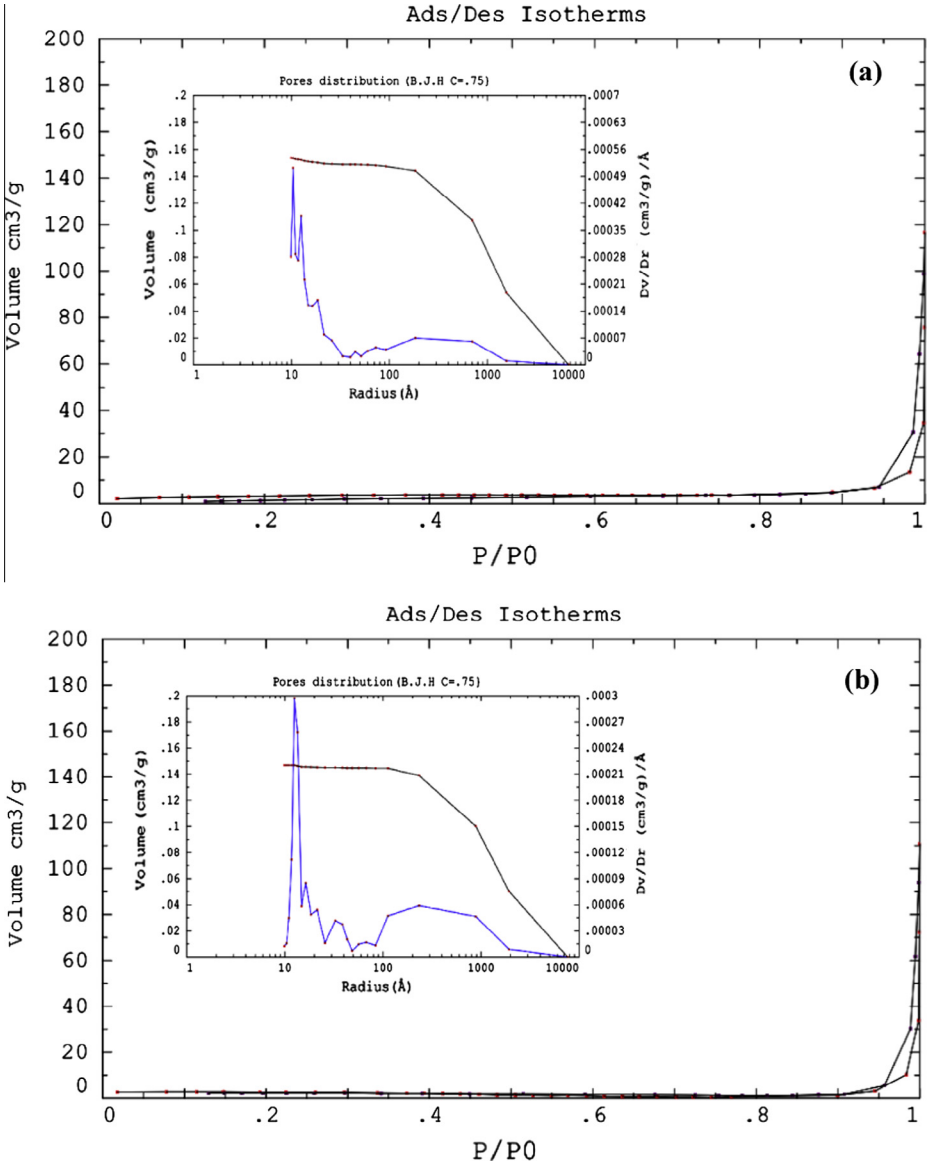

Figure 7 N_2 sorption isotherms and pore size distribution of (a) ICS and (b) ICS-SO_3H catalyst.

Table 2 Structural properties of ICS-SO_3H catalyst in comparison with other reported journals.

Catalyst	[a]Elemental analysis (wt.%)					[b]Acid sites density (mmol g^{-1})		[c]Surface area (m^2 g^{-1})	[c]Pore volume (cm^3 g^{-1})	[c]Average pore size (nm)	References
	C	H	N	O	S	Total	SO_3H				
ICS	77.4 ± 2.8	1.8 ± 0.3	–	20.8 ± 1.2	0.00	5.57 ± 0.8	0.00	10.54 ± 1.8	0.57 ± 0.05	53 ± 3.8	In this work
ICS-SO_3H	61.5 ± 3.1	3.4 ± 0.8	–	27.9 ± 2.1	9.20 ± 1.7	12.54 ± 2.6	6.97 ± 1.7	12.40 ± 2.1	0.51 ± 0.08	44 ± 2.6	In this work
Sulfonated-glucose catalyst	–	–	–	–	–	–	1.34	2	–	1.2	Mekhilef et al. (2011)
Sulfonated-cellulose catalyst	–	–	–	–	–	–	1.8	< 5	0.5	1.2–1.5	Okamura et al. (2006)
Sulfonated-waste vegetable oil asphalt	–	–	–	–	–	2.04	–	7.48	–	43.9	Okuhara (2002)
Sulfonated-lignin catalyst	–	–	–	–	–	1.71	0.86	4.7	–	–	Peng-Lim et al. (2012)

[a] The S content was determined by CHNOS elemental analysis.
[b] The total acid sites density was determined by NH_3-TPD.
[c] The surface and porosity's characteristics were calculated by BET surface area analysis.

The activation of ICS by thermal treatment with concentrated H_2SO_4 caused the surface area of the catalyst to increase from 10.54 m^2 g^{-1} to 12.40 m^2 g^{-1} as shown in Table 2 due to the small destruction on the carbon network producing the smaller particles. However, the average pore volume and pore size decreased slightly, suggesting that the SO_3H groups were incorporated inside the pores of the carbon catalyst (Lokman et al., 2015). These results are significant compared to the surface areas of glucose catalyst reported by Okamura et al. (2006) which was 2 m^2 g^{-1}, cellulose-based catalyst reported by Nakajima and Hara (2012) which was < 5 m^2 g^{-1}, and sulfonated-lignin catalyst by Guo et al. (2012) which was 4.7 m^2 g^{-1}.

Moreover, the acid density analysis shown in Table 2 reveals that the total acid density of macroporous ICS-SO_3H was 12.54 mmol g^{-1} with a total of —SO_3H group being 6.97 mmol g^{-1} higher than acid density glucose catalyst reported by Okamura et al. (2006) which was 1.34 mmol g^{-1}, sulfonated waste vegetable oil pitch reported by Shu et al. (2010) which was 2.04 mmol g^{-1}, and sulfonated lignin catalyst reported by Guo et al. (2012) which was 1.71 mmol g^{-1} of total acid density. The high concentration of acid density could be attributed from the larger surface area and bimodal porosity of meso- and macroporous which allowed large quantity of SO_3H group incorporated on carbon lattice. According to Lee et al. (2015) the catalytic activity of certain catalyst depends on the amount of active sites and the surface area of the catalyst. In this case, the ICS-SO_3H catalyst was expected to give high activity due to high total acid density generated on its aromatic carbon structure.

3.3. Catalytic activity of the ICS-SO_3H catalyst

In this study, the catalytic performance of the carbon-based solid acid catalyst was studied by varying the ranges of methanol-to-PFAD molar ratio, catalyst amount, reaction temperature and reaction time.

3.3.1. Effect of methanol-to-PFAD molar ratio

In the biodiesel production process, both transesterification and esterification require an optimum amount of methanol to shift the equilibrium to the high production of FAME yield. In this study, a series of reactions with different methanol-to-PFAD molar ratios (5, 10, 15, 20, and 25) were carried out to investigate their effect on the conversion of PFAD to methyl ester. The reaction was done with 2 wt.% of ICS-SO_3H catalyst at 75 °C for 3 h of reaction time. The conversion percentages of FFA to methyl ester versus methanol molar ratio are shown in Fig. 8(a). The FFA conversion increased with the increasing quantity of methanol. The conversion reached a value of above 90% with an addition of methanol molar ratio from 5 to 10, and it rose from 79.2% up to 94.7% of FFA conversion. The difference in conversion between both ratios was about 15.5%. The conversion slightly increased from 95% to 96.3% for 15, 20 and 25 of methanol molar ratio. It was discovered that, a further increase of the methanol molar ratio above 10 did not significantly increase the FFA conversion. As reported by Nakpong and Wootthikanokkhan (2010), the sustainability of the FFA conversion may be due to the effect of water formation during the esterification of FFA and also a small portion of water existed in the commercially grade

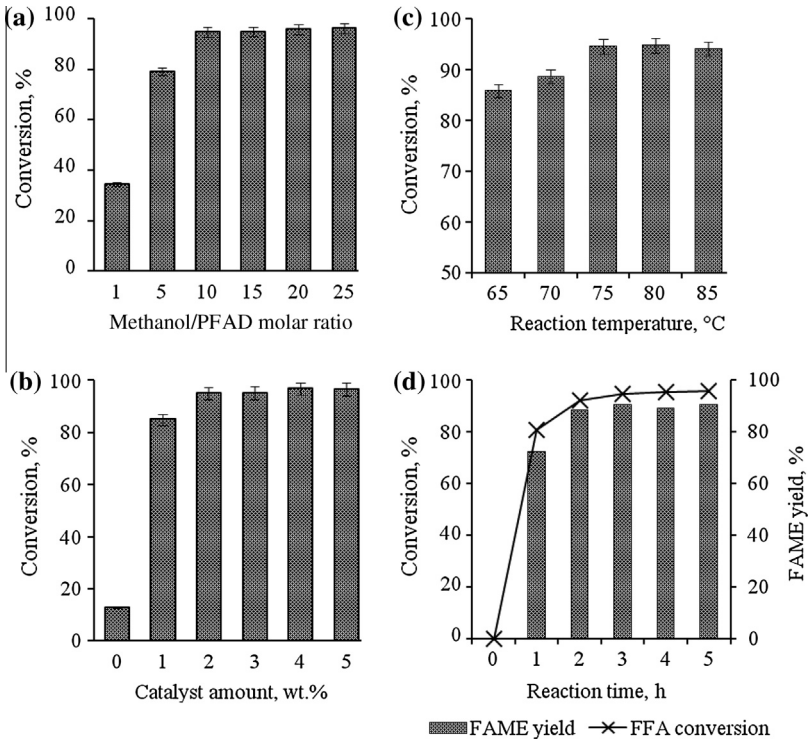

Figure 8 (a) Effect of methanol amount on FFA conversion of PFAD, (b) effect of catalyst amount on FFA conversion of PFAD, (c) effect of reaction temperature on FFA conversion of PFAD and (d) rate of FFA conversion and FAME yield at optimized condition.

methanol, which inhibited further reaction process. Therefore, the lowest methanol molar ratio that gave the FFA conversion over than 90% was 10, hence selected as the optimum methanol molar ratio and used for subsequent optimization studies.

3.3.2. Effect of the ICS-SO_3H catalyst amount

The loading effect of the macroporous ICS-SO_3H catalyst on esterification of PFAD was investigated with its amount varying from 1 to 5 wt.% (based on the weight of the feedstock). The operating reaction conditions (methanol-to-PFAD molar ratio of 10, reaction temperature of 75 °C, and reaction time 3 h) were kept constant throughout the reaction process. Fig. 8(b) shows the percentage of FFA conversion to methyl ester versus the quantity of the catalyst. The results revealed that the presence of 1 wt.% of ICS-SO_3H catalyst significantly increases the rate of conversion from 12.8% to 85%. The conversion was elevated equal to 94.9% with further addition of 2 wt.% of catalyst. However, an addition of 3–5 wt.% of catalyst showed no significant increment on the FFA conversion. Thus, 2 wt.% of ICS-SO_3H catalyst was adequate for esterification of PFAD. Konwar et al. (2014), produced biodiesel from acid oils using sulfonated carbon catalyst derived from oil cake waste. They managed to reduce the acid value of oils up to 97% using 5–6.5 wt.% of catalyst and 43:1 methanol-to-oil molar ratio at 80 °C for 8 h. However, these conditions resulted in the high cost of biodiesel production. Compared to our studies, the efficiency of the macroporous ICS-SO_3H catalyst was not only improved, but has also been proven ideal to be used for low-cost biodiesel production process.

3.3.3. Effect of reaction temperature

Fig. 8(c) shows the effect of reaction temperature on FAME conversion, conducted from 65 to 85 °C with catalyst amount of 2 wt.%, methanol-to-PFAD molar ratio of 10 and reaction time of 3 h. The conversion pattern revealed the increment of the reaction temperature starting from 65 to 70 °C increases the conversion of FFA to methyl ester from 85.8% to 88.6% and it was continued up to 94.6% as increased the temperature up to 75 °C. However, the results show insignificant increment of conversion when the reaction temperature was increased from 75 to 85 °C. As observed, the equilibrium conversion of fatty acids was achieved at 75 °C. According to Hayyan et al. (2010) the optimum reaction temperature can affect the reaction rate by increasing the kinetic energy to the maximum level to move the molecules faster during the esterification process. Therefore, it is easier to break the carbon bond in the fatty acid molecule structure when the process is supported by a specific amount of alcohol molecules and catalyst.

3.3.4. Rate of reaction

Fig. 8(d) shows the rate of FFA conversion and FAME yield for duration of 5 h, which were conducted at optimum reaction conditions (2 wt.% of catalyst, 10 of methanol-to-PFAD molar ratio and at 75 °C reaction temperature). The results revealed that the average FAME yield was lower compared to the percentage of the FFA conversion. The product yield was found to have increased to above 70% as the reaction was continued for 1 h. It seems that the other optimum conditions such as the catalyst, methanol and reaction temperature played an important role to ensure the conversion occurred at

maximum rate. After 3 h, the FFA conversion and FAME yield increased up to 94.6% and 89.7%, respectively. There was no increment shown for both FFA and FAME yield starting from 3 to 5 h. Chin et al. (2012) explained that the increment of the reaction temperature up to optimum level enhanced the improvement of the mass transfer limitation between reaction mixture and catalyst, which will lead to the increment of the reaction rate. At that point the equilibrium reaction was achieved where the maximum conversion could occur and gave high yield of biodiesel product.

3.4. Reusability and leaching analysis of ICS-SO_3H catalyst

In this work, the ICS-SO_3H catalyst was separated from the product mixture, washed and dried prior to next reaction cycle without catalyst reactivation step. The biodiesel product was collected at every reaction cycle to determine the FAME yield and sulfur content. Fig. 9 shows the reusability and leaching analysis of the catalyst over the reaction cycles. Results showed the declines of FAME yield from 90.4% at first cycle and 72.2% at sixth cycle. It was established that the FAME yield decreased in each cycle due to the losses or leaching of the —SO_3H groups from the catalyst. However, the concentration of the sulfur (assuming all the sulfur are from the —SO_3H groups) in the biodiesel product was less than 0.001 ppm. According to ASTM D6751 and EN14214 standard method, the maximum amount of sulfur in the fuel allowed for commercialization is 0.001 ppm. Thus, the produced biodiesel derived from PFAD was acceptable for commercialization. The recycle ability and low leaching of active sites can be explained by the majority of the active sites that were incorporated inside the meso- and macro-pores of the catalyst. Guo et al. (2012) studied the deactivation of the macroporous carbon-based solid acid catalyst derived from lignin. They mentioned that the deactivation of the catalyst was mainly caused by the leaching of the acid sites (—SO_3H) in methanol phase. In their case, the conversion of FFA dropped to 67.8% with reduction of —SO_3H amount about 8.5% after four reaction cycles.

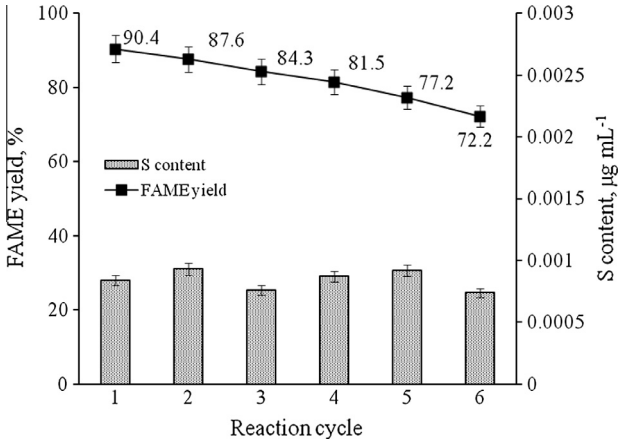

Figure 9 Reusability and leaching analysis of ICS-SO_3H catalyst. Reaction conditions: catalyst amount 2 wt.%, methanol-to-PFAD molar ratio 10, reaction temperature 75 °C, and reaction time 3 h.

3.5. PFAD biodiesel profile

FAME content of PFAD biodiesel produced from the reaction was analyzed by GC–MS spectrometer as shown in Supp. 1. It was observed that 5 major FAME constituents (e.g., methyl myristate, methyl palmitate, methyl linoleate, methyl oleate, and methyl stearate in ascending order of the polarity properties) existed in the PFAD biodiesel product. A previous investigation also demonstrated the appearance of 5 major peaks of FAME components in the PFAD biodiesel (Lokman et al., 2014b).

The FTIR spectrum of PFAD biodiesel is presented in Supp. 2. The peak at 2931 cm^{-1} showed the transmittance assigned to alkyl (—CH) stretching modes. The prominent peak observed at 1741 cm^{-1} attributed to the carbonyl (C═O stretch) from the ester. Meanwhile, one obvious peak observed at 1180 cm^{-1} was assigned for C—O from ester (Rashid et al., 2011a,b).

4. Conclusions

In the present work, the preparation of the meso- and macroporous carbon-based catalyst from starch, as well as their catalytic activity performance in esterification of PFAD oil with methanol is reported. The effect of the porous carbon based catalyst, which provides more anchor for acid active sites attachment was discussed. The characterization results show that the ICS-SO_3H catalyst exhibits larger surface area of 12.4 $m^2 g^{-1}$, bimodal porosity with average pore size of 44 nm and the total acid sites density of 12.54 mmol g^{-1}. It was concluded that, the presence of bimodal meso- and macroporous ICS-SO_3H catalyst efficiently increases the density of active sites. The performance of prepared catalyst and the effect of operating conditions on esterification of PFAD were investigated. It revealed that, the FFA conversion and FAME yield achieved 94.6% and 90.4% respectively at the following reaction conditions: quantity of ICS-SO_3H catalyst 2 wt.%, methanol-to-PFAD molar ratio of 10:1, reaction temperature of 75 °C and reaction time of 3 h. The ICS-SO_3H catalyst was successfully recycled up to 6 times with minimal leaching of active sites. As a result, the sulfur content in the product did not exceed the maximum limit allowed by ASTM and EN standards. The analysis of biodiesel produced was in good agreement with the previous reported literature.

Acknowledgments

Authors would like to thank Ministry of Science, Technology and Innovation (MOSTI), Malaysia for eScience funds (Vot. No. 5450746; Project No. 06-01-04-SF1780). Thanks to Universiti Teknologi MARA and Malaysia's Ministry of Higher Education as well for giving a scholarship to one of the authors (Ibrahim M. Lokman).

Appendix A. Supplementary material

Supplementary data associated with this article can be found, in the online version, at http://dx.doi.org/10.1016/j.arabjc.2015.06.034.

References

Alhassan, F.H., Yunus, R., Rashid, U., Sirat, K., Islam, A., Lee, H.V., Taufiq-Yap, Y.H., 2013. Production of biodiesel from mixed vegetable oils using Ferric hydrogen sulphate as an effective reusable heterogeneous solid acid catalyst. Appl. Catal. A – Gen. 456, 182–187.

Ashnani, M.H.M., Johari, J., Hashim, H., Hasani, E., 2014. A source of renewable energy in Malaysia, why biodiesel? Renew. Sustain. Energy Rev. 35, 244–257.

Atadashi, I.M., Aroua, M.K., Abdul Aziz, A.R., Sulaiman, N.M.N., 2012. Production of biodiesel using high free fatty acid feedstocks. Renew. Sustain. Energy Rev. 16, 3275–3285.

Badday, A.S., Abdullah, A.Z., Lee, K.T., 2013. Optimization of biodiesel production process from Jatropha oil using supported heteropolyacid catalyst and assisted by ultrasonic energy. Renew. Energy 50, 427–432.

Chin, L.H., Abdullah, A.Z., Hameed, B.H., 2012. Sugar cane bagasse as solid catalyst for synthesis of methyl esters from palm fatty acid distillate. Chem. Eng. J. 183, 104–107.

Cho, H.J., Kim, J.-K., Ahmed, F., Yeo, Y.-K., 2013. Life-cycle greenhouse gas emissions and energy balances of a biodiesel production from palm fatty acid distillate (PFAD). Appl. Energy 111, 479–488.

Dashmane, C.A., Wright, M.W., Lachgar, A., Rohlfing, M., Liu, Z., Le, J., Hanson, B.E., 2013. A comparative study of solid carbon acid catalysts for the esterification of free fatty acids for biodiesel production: evidence for leaching of colloidal carbon. Bioresour. Technol. 147, 597–604.

Fratzl, P., Weinkamer, R., 2007. Nature's hierarchical materials. Prog. Mater. Sci. 52, 1263–1334.

Guo, F., Xiu, Z.-L., Liang, Z.-X., 2012. Synthesis of biodiesel from acidified soybean soapstock using a lignin-derived carbonaceous catalyst. Appl. Energy 98, 47–52.

Hayyan, A., Alam, M.Z., Mirghani, M.E.S., Kabbashi, N.A., Hakimi, N.I.N.M., Siran, Y.M., Tahiruddin, S., 2010. Sludge palm oil as a renewable raw material for biodiesel production by two-step processes. Bioresour. Technol. 101, 7804–7811.

Islam, A., Taufiq-Yap, Y.H., Chu, C.-M., Chan, E.-S., Ravindra, P., 2013. Studies on design of heterogeneous catalysts for biodiesel production. Process Saf. Environ. 91, 131–144.

Kim, J.H., Fang, B., Kim, M.-S., Yoon, S.B., Bae, T.-S., Ranade, D.R., 2010. Facile synthesis of bimodal porous carbon as an anode catalyst support in proton exchange membrane fuel cell. Electrochim. Acta 55, 7628–7633.

Konwar, L.J., Das, R., Thakur, A.J., Salminen, E., Mäki-Arvela, P., Kumar, N., Mikkola, J.-P., Deka, D., 2014. Biodiesel production from acid oils using sulfonated carbon catalyst derived from oil-cake waste. J. Mol. Catal. A – Chem. 388–389, 167–176.

Lee, H.V., Juan, J.C., Taufiq-Yap, Y.H., 2015. Preparation and application of binary acid-base $CaO–La_2O_3$ catalyst for biodiesel production. Renew. Energy 74, 124–132.

Lee, H.V., Yunus, R., Juan, J.C., Taufiq-Yap, Y.H., 2011. Process optimization design for jatropha-based biodiesel production using response surface methodology. Fuel Process. Technol. 92, 2420–2428.

Liu, W., Yin, P., Liu, X., Chen, W., Chen, H., Liu, C., Qu, R., Xu, Q., 2013. Microwave assisted esterification of free fatty acid over a heterogeneous catalyst for biodiesel production. Energy Convers. Manage. 76, 1009–1014.

Lokman, I.M., Rashid, U., Yunus, R., Taufiq-Yap, Y.H., 2014a. Carbohydrate-derived solid acid catalysts for biodiesel production from low-cost feedstocks: a review. Catal. Rev: Sci. Eng. 56, 187–219.

Lokman, I.M., Rashid, U., Taufiq-Yap, Y.H., Zainal, Z., 2014b. Microwave-assisted biodiesel production by esterification of palm fatty acid distillate. J. Oleo. Sci. 63, 849–855.

Lokman, I.M., Rashid, U., Yunus, R., Taufiq-Yap, Y.H., 2015. Methyl ester production from palm fatty acid distillate using sulfonated glucose-derived acid catalyst. Renew. Energy 81, 347–354.

Lou, W.-Y., Zong, M.-H., Duan, Z.-Q., 2008. Efficient production of biodiesel from high free fatty acid-containing waste oils using various carbohydrate-derived solid acid catalysts. Bioresour. Technol. 99, 8752–8758.

Mekhilef, S., Siga, S., Saidur, R., 2011. A review on palm oil biodiesel as a source of renewable fuel. Renew. Sustain. Energy Rev. 15, 1937–1949.

Nakajima, K., Hara, M., 2007. Environmentally benign production of chemicals and energy using a carbon based strong solid acid. J. Am. Ceram. Soc. 90, 3725–3734.

Nakajima, K., Hara, M., 2012. Amorphous carbon with SO_3H groups as a solid Brønsted acid catalyst. ACS Catal. 2, 1296–1304.

Nakpong, P., Wootthikanokkhan, S., 2010. High free fatty acid coconut oil as a potential feedstock for biodiesel production in Thailand. Renew. Energy 35, 1682–1687.

Okamura, M., Takagaki, A., Toda, M., Kondo, J.N., Domen, K., Tatsumi, T., Hara, M., Hayashi, S., 2006. Acid-catalyzed reactions on flexible polycyclic aromatic carbon in amorphous carbon. Chem. Mater. 18, 3039–3045.

Okuhara, T., 2002. Water-tolerant solid acid catalyst. Chem. Rev. 102, 3641–3666.

Ormsby, R., Kastner, J.R., Miller, J., 2012. Hemicellulose hydrolysis using solid acid catalyst generated from biochar. Catal. Today 190, 89–97.

Peng-Lim, B., Ganesan, S., Maniam, G.P., Khairuddean, M., 2012. Sequential conversion of high free fatty acid oils into biodiesel using a new catalyst system. Energy 46, 132–139.

Ping, B.T.Y., Yusof, M., 2009. Characteristics and properties of fatty acid distillates from palm oil. Oil Palm Bull. 5, 5–11.

Rashid, U., Anwar, F., Ashraf, M., Saleem, M., Yusup, S., 2011a. Application of response surface methodology for optimizing transesterification of *Moringa oleifera oil*: biodiesel production. Energy Convers. Manage. 52, 3034–3042.

Rashid, U., Anwar, F., Knothe, G., 2011b. Biodiesel from Milo (*Thespesia populnea L.*) seed oil. Biomass Bioenergy 35, 4034–4039.

Reynolds, D.B., 2014. World oil production trend: comparing Hubbert multi-cycle curves. Ecol. Econ. 98, 62–71.

Shu, Q., Gao, J., Nawaz, Z., Liao, Y., Wang, D., Wang, J., 2010. Synthesis of biodiesel from waste vegetable oil with large amounts of free fatty acids using carbon-based solid acid catalyst. Appl. Energy 87, 2589–2596.

Stein, A., Li, F., Denny, N.R., 2008. Morphological control in colloidal crystal templating of inverse opals, hierarchical structures, and shaped particles. Chem. Mater. 20, 649–666.

Takagaki, A., Toda, M., Okamura, M., Kondo, J.N., Hayashi, S., Domen, K., Hara, M., 2007. Esterification of higher fatty acids by a novel strong solid acid. Catal. Today 116, 157–167.

Taufiq-Yap, Y.H., Lee, H.V., Hussein, M.Z., Yunus, R., 2011. Calcium-based mixed oxide catalysts for methanolysis of Jatropha curcas oil to biodiesel. Biomass Bioenergy 35, 827–834.

Valle-Vigón, P., Sevilla, M., Fuerters, A.B., 2012. Sulfonated mesoporous silica–carbon composites and their use as solid acid catalysts. Appl. Surf. Sci. 261, 574–583.

Walcarius, A., Collinson, M.M., 2009. Analytical chemistry with silica sol–gels: traditional routes to new materials for chemical analysis. Annu. Rev. Anal. Chem. 2, 121–143.

Wang, C., Hu, Y., Chen, Q., Lv, C., Jia, S., 2013. Bio-oil upgrading by reactive distillation using p-toluene sulfonic acid catalyst loaded on biomass activated carbon. Biomass Bioenergy 56, 405–411.

Yu, H., Jin, Y., Li, Z., Peng, F., Wang, H., 2008. Synthesis and characterization of sulfonated single-walled carbon nanotubes and their performances as solid acid catalyst. J. Solid State Chem. 181, 432–438.

Zhang, J., Wang, K., Guo, S., Wang, S., Liang, Z., Chen, Z., Fu, J., Xu, Q., 2014. One-step carbonization synthesis of hollow carbon nanocoons with multimodal pores and their enhanced electrochemical performance for supercapacitors. Appl. Mater. Interfaces 6, 2192–2198.

Zhang, M., Sun, A., Meng, Y., Wang, L., Jiang, H., Li, G., 2015. High activity ordered mesoporous carbon-based solid acid catalyst for the esterification of free fatty acids. Micropor. Mesopor. Mater. 204, 210–217.

Zhao, B., Collinson, M.M., 2010. Well-define hierarchical templates for multimodal porous material fabrication. Chem. Mater. 22, 4312–4319.

Zong, M.-H., Duan, Z.-Q., Lou, W.-L., Smith, T.J., Wu, H., 2007. Preparation of a sugar catalyst and its use for highly efficient production of biodiesel. Green Chem. 9, 434–437.